Materials Science & Engineering C 125 (2021) 112108

Contents lists available at ScienceDirect

Materials Science & Engineering C

journal homepage: www.elsevier.com/locate/msec

Antimicrobial and enzyme-responsive multi-peptide surfaces for bone-anchored devices

Nicholas G. Fischer [a], Xi Chen [a], Kristina Astleford-Hopper [b], Jiahe He [a], Alex F. Mullikin [a], Kim C. Mansky [b], Conrado Aparicio [a,*]

[a] MDRCBB-Minnesota Dental Research Center for Biomaterials and Biomechanics, University of Minnesota, Moos Tower, 515 Delaware St. SE, Minneapolis, MN 55455, USA

[b] Department of Diagnostic and Biological Sciences, University of Minnesota, Moos Tower, 515 Delaware St. SE, Minneapolis, MN 55455, USA

ARTICLE INFO

Keywords:
Multifunctional surface
Implant
Antimicrobial peptide
Osteoclasts
MMP
Antimicrobial
Stimuli-responsive

ABSTRACT

Functionalization of dental and orthopedic implants with multiple bioactivities is desirable to obtain surfaces with improved biological performance and reduced infection rates. While many approaches have been explored to date, nearly all functionalized surfaces are static, i.e., non-responsive to biological cues. However, tissue remodeling necessary for implant integration features an ever-changing milieu of cells that demands a responsive biomaterial surface for temporal synchronization of interactions between biomaterial and tissue. Here, we successfully synthesized a multi-functional, dynamic coating on titanium by co-immobilizing GL13K antimicrobial peptide and an MMP-9 – a matrix metalloproteinase secreted by bone-remodeling osteoclasts – responsive peptide. Our co-immobilized peptide surface showed potent anti-biofilm activity, enabled effective osteoblast and fibroblast proliferation, and demonstrated stability against a mechanical challenge. Finally, we showed peptide release was triggered for up to seven days when the multi-peptide coatings were cultured with MMP-9-secreting osteoclasts. Our MMP-9 cleavable peptide can be conjugated with osteogenic or immunomodulatory motifs for enhanced bone formation in future work. Overall, we envisage our multifunctional, dynamic surface to reduce infection rates of percutaneous bone-anchored devices via strong anti-microbial activity and enhanced tissue regeneration via temporal synchronization between biomaterial cues and tissue responses.

1. Introduction

Long-term implant fate is dictated by a "race" between microbial colonization of the implant surface and tissue integration [1]. Bacterial colonization of implant surfaces can lead to biofilm formation and hamper cellular adhesion and tissue integration [2]. Rapid wound healing and peri-implant bone regeneration could both reduce healing times and infection [3]. Unfortunately, the generally bio-inert nature of titanium (Ti; still the most widely-used material for manufacturing dental and orthopedic implants due to its excellent mechanical properties, chemical stability, and biocompatibility) [4–6] has no ability to harness the host's immune system, is not beneficial to osteoprogenitors and hinders rapid bone formation, and favors biofilm formation [7,8]. Titanium's lack of bioactivity contributes to the failure rates for orthopedic and dental implants, which comprehensive meta-analyses suggest place at 12.2% and 17%, respectively [9,10]. High failure rates combined with increasing number of implants placed each year – the prevalence of dental implants could be as high as 23% of the entire adult US population by 2026 – motivates the development of new materials capable of increasing long-term success rates [11].

Functionalization of implant surfaces with bioactive molecules offers a tempting solution for overcoming slow peri-implant bone regeneration via immunomodulation, presentation of cell-instructive cues, and prevention of biofilm formation [12–14]. A variety of bioactive molecules including proteins [15–19], nucleotides [20,21], peptides [22–24], and antimicrobial agents [25–27] have been immobilized to functionalize titanium implants. However, these coatings typically display a single biofunction, which may not offer sufficient simultaneous or sequentially-controlled concerted relief against biofilm formation and slow bone regeneration. A related, pernicious problem is that some bioactive molecules facilitating enhanced osteoprogenitor activity are also highly-stimulative for adhesion of bacteria compared to bare

* Corresponding author at: MDRCC-Minnesota Dental Research Center for Biomaterials and Biomechanics, University of Minnesota, 16-250A Moos Tower, 515 Delaware St. SE, Minneapolis, MN 55455, USA.
E-mail address: apari003@umn.edu (C. Aparicio).

https://doi.org/10.1016/j.msec.2021.112108
Received 4 January 2021; Received in revised form 19 March 2021; Accepted 10 April 2021
Available online 16 April 2021

titanium [28]. One pertinent example is fibronectin - an extracellular matrix protein commonly used to improve cell attachment - that expresses a binding domain against *Staphylococci* spp. [29] A multifunctional coating with the ability to enhance cellular responses and simultaneously inhibit biofilm formation would be beneficial toward reducing implant infection rates.

Another drawback of existing implant surface functionalization methods - and implants as a whole - is they do not respond to physiological cues; implant surfaces themselves are static. This has been widely recognized for 3-dimensional tissue scaffolds, and as a result, a range of materials responsive to internal or external stimuli such as pH, ionic strength, magnetism, or enzymes have been developed [30–32]. However, this approach has been scarcely explored for biomaterial surfaces; indeed, the traditional paradigm for biomaterial surfaces is stability [33,34] with the notable exception of thermoresponsive surfaces for cell sheet production [35,36]. Static surfaces are in opposition to bone remodeling and implant site healing where an ever-changing milieu of osteoprogenitor and immune cells demands a responsive biomaterial surface [37,38]. As a result, dynamic implant surfaces for bone regeneration would be advantageous for synchronization of activity of biomaterial cues that would accelerate tissue responses.

Here, we co-immobilized oligopeptides to obtain a multi-functional dynamic surface toward the long-term goal of reducing bone-anchored, transdermal, dental, and orthopedic implant failure. First, we selected an antimicrobial peptide (AMP), GL13K, derived from the human salivary Parotid Secretory Protein (BPIFA2) [39]. AMPs generally feature low host cytotoxicity, low bacterial resistance, and broad spectrum activity against Gram negative and Gram positive bacteria, fungi, and viruses [40,41]. Second, we selected a matrix metalloprotease 9 (MMP-9) cleavable peptide (MMP9-CP) [42]. MMPs are zinc-dependent proteases responsible for degradation of extracellular matrix (ECM) components including collagen, fibronectin, and various proteoglycans during normal remodeling and repair processes [43,44]. MMP cleavable sequences have been applied in bio-degradable scaffolds for tissue engineering and regenerative medicine [45,46]. including MMP-9 sensitive sequences [47,48]. However, the covalent immobilization of MMP cleavable peptides on solid substrates for the purpose of controlled release of bioactive motifs has been much less investigated [49,50].

MMP-9 is highly expressed and involved in osteoclast-mediated bone remodeling and during initial implant site clearing, as well as secreted by inflammatory cells such as neutrophils, macrophages, and B-lymphocytes [51–53]. This expression profile make the selected MMP9-CP an excellent candidate for enzyme-mediated release since the stimuli (MMP-9 expression) would be a physiologically-normal inflammatory reaction or remodeling process when tissue healing and bone formation after surgical implantation is most active [54]. MMP9-CP can be easily coupled with bone regenerative peptides [55,56] or immunomodulatory motifs [57] in the future to build a multifunctional coating with combined antimicrobial and enhanced bone regeneration and healing activity triggered by active bone remodeling.

Here, we demonstrate in vitro that a multi-functional, dynamic surface composed of co-immobilized AMP and MMP9-CP showed simultaneous strong antimicrobial activity against an early colonizer of oral surfaces and responsiveness to enzymatic activity mediated by protease secretion from osteoclasts.

2. Material and methods

2.1. Fabrication of multi-peptide coatings

Peptide coatings on Ti surfaces were prepared through a three step method. Ti was first activated by NaOH etching and then silanized using (3-chloropropyl)triethoxysilane (CPTES). Immobilization of mono or co-immobilized coatings on CPTES-modified Ti surfaces was then performed as we have described [23,58,59].

Commercially pure titanium Grade II discs (McMaster-Carr) were ground, polished, and soaked in 5 M NaOH overnight at 60 °C to form reactive –OH groups on Ti surfaces (eTi group). Samples were then placed in 7 mL anhydrous pentane, 1.2 mL (3-chloropropyl)triethoxysilane (CPTES; Sigma-Aldrich) and 0.6 mL diisopropylethylamine (DIEA; Sigma-Aldrich). Periodic two minute ultrasonication cycles were applied every ten minutes for one hour. GL13K and MMP9-CP peptides (purity>98%) were synthesized by solid-phase peptide synthesis and purchased from AAPPTec (Louisville, KY). Covalent immobilization of peptides was accomplished by immersing silanized Ti discs into a mixed solution with 0.1 mM GL13K (GKIIKLKASLKLL-NH_2) and 0.1 mM MMP9-CP (KKGGGPLGMYS) in 0.5 mg/mL Na_2CO_3 overnight as described below. The two additional lysines and three glycines in MMP9-CP were used to promote surface orientation at the N-terminus and as spacers, respectively [24,60].

The effect of synthesis conditions on co-immobilization was assessed; namely, solution pH and sequential or simultaneous addition of peptides. Our purpose was to systemically discern reaction conditions that favored a balanced surface ratio of each peptide on the surface (i.e., obtain surface multifunctionality). Ti samples were treated with three different treatments: 1) silanized Ti disc were submerged in a solution of GL13K for 3.5 h (pre-immobilized with GL13K), followed by adding MMP9-CP peptide and co-immobilizing overnight; 2) silanized Ti discs were submerged in MMP9-CP solution for 3.5 h (pre-immobilized with MMP9-CP), followed by adding GL13K peptide and co-immobilizing overnight; 3) silanized Ti discs were submerged in a solution of mixed GL13K and MMP9-CP (1:1 by mole) peptides and simultaneously co-immobilized with the two peptides overnight. Three pHs (9.5, 10.5, and 11.5) for peptide immobilization were tested for each treatment (3 treatment groups × 3 pH groups yielding 9 total groups) to obtain different surface ratios of GL13K and MMP9-CP. Ti surfaces functionalized with only one of the two peptide - GL13K (mono-immobilized GL13K group) or MMP9-CP (mono-immobilized MMP9-CP group) - were prepared by submerging silanized Ti discs in GL13K only or MMP9-CP only solution (both at pH = 9.5) overnight as controls.

2.2. Selection of best peptide co-immobilization condition

Fluorescently labeled GL13K-FAM and MMP9-CP-TAMRA (>95% purity) were covalently immobilized on Ti surface alone (mono-immobilized GL13K and mono-immobilized MMP9-CP groups) or combined under different co-immobilization conditions (9 total experimental conditions plus 2 mono-immobilized controls) as described above. Samples were collected after immobilization, rinsed with distilled water and acetone, and the fluorescence signal on surfaces were measured with a Synergy TM 2 multi-mode microplate reader (BioTek). GL13K signal intensity was measured as surface optical density (OD) value at a wavelength of 485/528 nm and MMP9-CP was read at 575/620 nm. Surface fluorescence were also observed under a multi-channel fluorescent microscope (Eclipse E800, Nikon). Three samples were used per group.

2.3. X-ray photoelectron spectroscopy (XPS)

XPS was performed (SSX-100, Al Kα x-ray, 1 mm spot size, 35° take-off angle) to characterize the atomic composition of the surface. Survey scans (0–1100 binding energy, 4 scans/sample) were done at a 1 eV step-size. The peak fittings and semi-quantification of surface chemical composition were conducted using ESCA 2005 software provided with the XPS system.

2.4. Mechanical stability of the coatings

The surface prepared under best co-immobilization condition (surface pre-immobilized with GL13K, pH = 9.5 (Mixture group); selection rationalization described in Results) and mono-immobilized MMP9-CP

were mechanically-challenged by ultrasonication in deionized water for 2 h and incubated for one week in deionized water at 37 °C. Fluorescence visualization of the surfaces was performed with fluorescence microscopy (Leica DM6 B) and quantified using ImageJ (NIH, USA). Control eTi served as a background control. Three samples, with three micrographs taken per sample, were used per group.

2.5. Antimicrobial activity of the coatings

Streptococcus gordonii M5 was inoculated in 2 mL Bacto Todd-Hewitt broth (BD Biosciences). This overnight culture was diluted ten-fold with 0.9% NaCl and then fifty-fold with Todd-Hewitt broth. Four groups of Ti discs (eTi, GL13K coated Ti, MMP9-CP coated Ti and Mixture peptide coated Ti; three samples per group) were placed under UV for ten minutes and then placed into a 48-well plate. One mL of the diluted culture was added to each well and incubated at 37 °C under mild shaking for 24 h. The discs were then removed and carefully rinsed with 1 mL NaCl solution three times. The discs were transferred to a new 48-well plate and incubated for additional two hrs. After incubation, Ti discs were thoroughly rinsed with 0.9% NaCl to remove loosely attached bacteria and then sonicated in 300 μL NaCl for 10 min to collect adhered bacteria on the surface. One hundred μL of the collected solution was mixed with 100 μL of the BacTiter-Glo™ Microbial Cell Viability kit (Promega) in an opaque 96-well plate. After five minutes of incubation at 37 °C, the luminescence was measured by a microplate luminometer (BioTek). Another 100 μL of collected solution was used for measuring colony-forming units (CFU). Briefly, 100 μL of the obtained solution was diluted serially 10, 100, 1000 and 10,000-fold. Then, 10 μL of solutions at each concentration were plated on Todd-Hewitt Agar plates and incubated overnight at 37 °C in a humidified atmosphere of 5% CO_2. The number of CFU was then quantified.

2.6. Evaluation of coating cytocompatibility

MC3T3-E1 murine pre-osteoblast cells (ATCC CRL-2593) were grown in MEM-α complete medium containing 10% fetal bovine serum and 1% penicillin-streptomycin (all Thermo Fisher Scientific). NIH-3 T3 murine fibroblast cells (ATCC CRL-1658) were grown in DMEM medium 10% fetal bovine serum, and 1% penicillin-streptomycin (all Thermo Fisher Scientific). Media was changed in the wells every 48 h. MC3T3 murine osteoblast cells and NIH3T3 fibroblast cells were seeded on eTi, Mixture, and tissue culture polystyrene control surfaces (TCPS) and MTT (3-(4, 5-dimethylthiazolyl-2)-2, 5-diphenyltetrazolium bromide) assays (Thermo Fisher Scientific) were performed after 24, 72 and 168 h of culture. Samples were measured at 570 nm to determine cell metabolic activity (proliferation) [61]. Five samples for each group were taken at each time interval. Substrates were also washed with phosphate buffered saline (PBS) and fixed with 4% paraformaldehyde for 10 min at room temperature after 24 and 120 h. Nuclei were stained with DAPI and observed using a fluorescence microscope (Eclipse E800, Nikon, Japan).

2.7. MMP-9 cleavable peptide release with osteoclast secreted MMP-9

2.7.1. Primary osteoclast culture

C57BL/6 (wild type; WT) mice were obtained from Jackson Laboratory, Bar Harbor, ME, USA. The use and care of these mice were reviewed and approved by the University of Minnesota Institutional Animal Care and Use Committee, IACUC protocol number 1806A36053. Tibiae and femora were dissected from WT mice and adherent tissue was removed. Primary bone marrow macrophages were isolated by flushing the bone marrow from the tibiae and femora. Red blood cell lysis buffer (150 mM NH_4Cl, 10 mM $KHCO_3$, 0.1 mM EDTA, pH = 7.4), was used to lyse red blood cells from the flushed bone marrow. The resulting cells were then plated in 10 cm tissue culture dishes (TPP, MidSci) and cultured overnight in osteoclast media (phenol red-free alpha-MEM (Gibco), 400 mM L-Glutamine (Invitrogen), 25 units/mL penicillin/streptomycin (Invitrogen), and with 5% (by volume) heat inactivated fetal bone serum (Atlanta Biologicals) and supplemented with 1.5% CMG 14–12 [culture supernatant containing M-CSF (macrophage stimulating colony-stimulating factor); Dr. Sunao Takeshita, Nagoya City University, Nagoya, Japan] [62]. Non-adherent cell populations, including osteoclast precursor cells, were removed and replated on top of bone slices placed in transwell inserts (Corning) at a concentration of 1×10^5 cells per well in osteoclast media supplemented with 1.5% CMG culture supernatant; MMP9-CP or Mixture surfaces were in the bottom portion of the well (one disc per well). Cells were refed every two days with osteoclast media containing 1.5% CMG plus 10 ng/mL of RANKL (R&D Systems) to initiate osteoclast differentiation for up to 7 days [63].

2.7.2. Immunofluorescence of MMP-9

To visualize protein expression of MMP-9 in osteoclasts, cells that were grown on the bone slices were fixed in 4% paraformaldehyde for 20 min following 7 days in culture. The cells were then washed with PBS, and permeabilized in PBS/0.3% Triton X-100 for 5 min. Discs were then blocked in immunofluorescence buffer (3% BSA, 20 mM $MgCl_2$, 0.3% Tween-20 in PBS) for 20 min and incubated at 4 °C with an MMP-9 (Abcam, ab38898) primary antibody for 3.5 h in immunofluorescence buffer. MMP-9 antibody was used 1:40. Cells were then washed three times for 5 min with PBS/0.1% Triton X-100. Cells were then incubated for 1.5 h with an Alexa-conjugated secondary antibodies at 1:200 (Invitrogen, A21428). Cells were then again washed three times for 5 min with PBS/0.1% Triton X-100. Cells were stained with DAPI, washed with PBS and bone slices were placed on glass slides for imaging. Images were obtained using an Olympus BX51 microscope.

2.7.3. Evaluation of MMP-9 cleaving activity of co-immobilized coatings with osteoclasts

A 40 μL aliquot of osteoclast media was taken each day after plating and read on a platereader at 575/620 nm (corresponding to MMP9-CP-TAMRA, where the fluorophore may function as mock, conjugated cargo for release) for Mixture and mono-immobilized MMP9-CP. In parallel, ten-fold dilutions of neat MMP9-CP in osteoclast media were incubated and read at each timepoint along with the aliquot. An individual standard curve (MMP9-CP in culture media) was read at each timepoint to determine MMP9-CP release taking into account possible changes in fluorescence signal strength associated with incubation in solution for extended times [64]. Fluorescence background was subtracted by having an additional set of mono-immobilized MMP9-CP and Mixture surfaces cultured without osteoclast (i.e., without MMP-9). Finally, release since the last timepoint (i.e., new release) was determined taking media changes or lack thereof since the last timepoint into account. Three samples were used per condition; this experiment was performed twice.

2.8. Statistical analysis

Statistically significant differences among groups were assessed using a one-way ANOVA with a Dunnett post hoc test for antimicrobial activity (control: eTi). A one-way ANOVA with a Tukey post hoc test was used for MTT metabolic activity within each time point. A Student's *t*-test was used to compare proliferation within each time point and to compare MMP9-CP osteoclast-mediated release within each time point. A Student's t-test was also used to compare MMP9-CP mono-immobilized fluorescent intensity after challenges compared to Mixture MMP9-CP. Statistical significance for all tests was assessed at $p < 0.05$.

3. Results and discussion

3.1. Fabrication of multi-peptide coatings

Co-immobilized biofunctionalized Ti surfaces were obtained through a three-step method (etching/surface activation + silanization/coupling

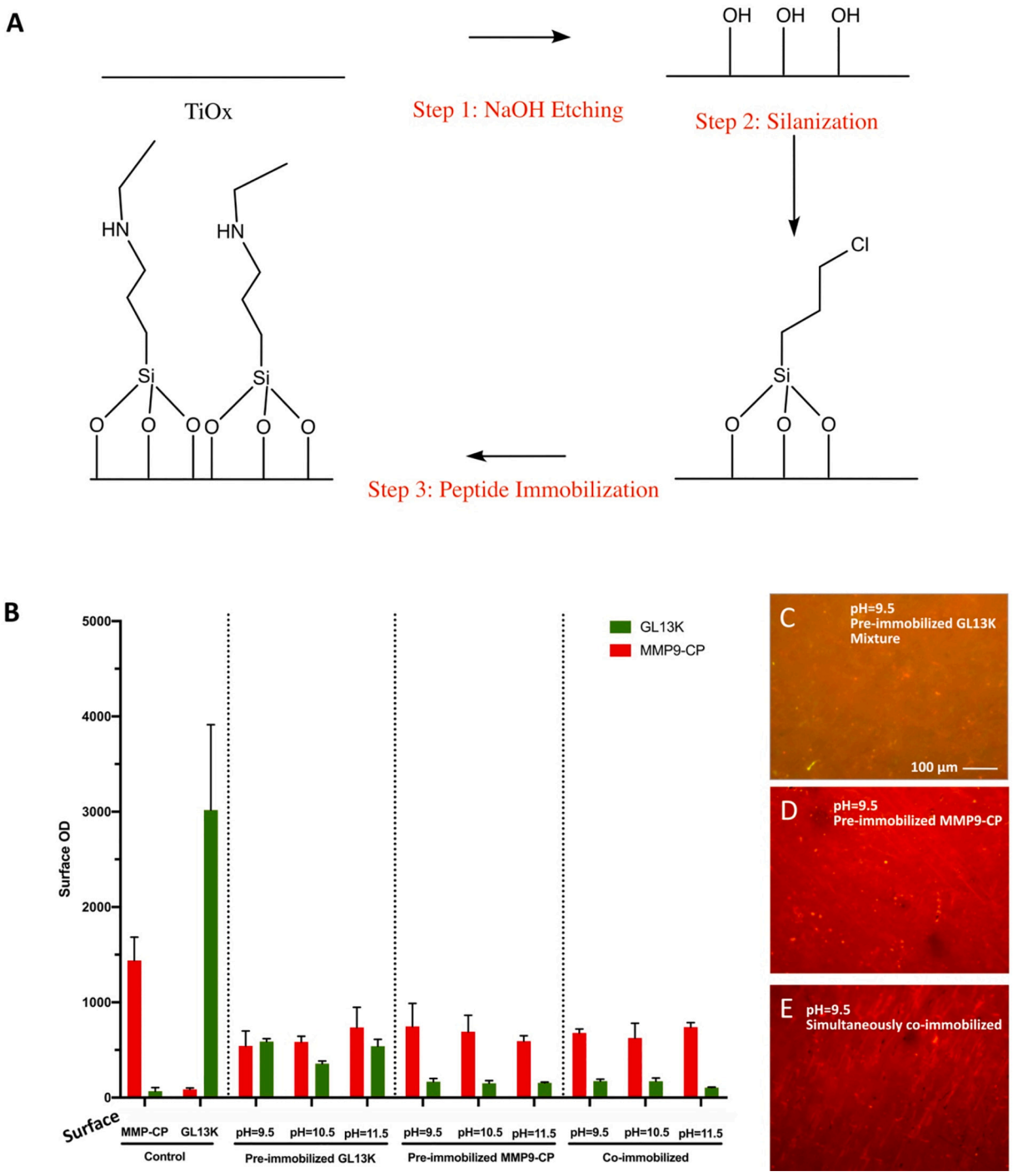

Fig. 1. Reaction scheme and fluorimetry of co-immobilized peptide surfaces and mono-peptide control surfaces. (A) Reaction scheme showing the chemical route of three-step immobilization. (B) OD values of fluorescently-labeled GL13K (green) and MMP9-CP (red) peptides on mono-immobilized MMP9-CP surfaces; mono-immobilized GL13K surfaces; pre-immobilized GL13K at three pHs (pH = 9.5, 10.5, and 11.5); pre-immobilized MMP9-CP at three pHs; and simultaneous co-immobilization at three pHs. Merged channel fluorescence micrographs of co-immobilized peptides for (C) pre-immobilized GL13K at pH = 9.5 ('Mixture' coating in following Figures), (D) pre-immobilized MMP9-CP at pH = 9.5, and (E) simultaneously co-immobilized at pH = 9.5. (For interpretation of the references to colour in this figure legend, the reader is referred to the web version of this article.)

agent + peptide tethering) using CPTES as a coupling agent (Fig. 1A). CPTES enabled the final covalent bonding of the peptides to the silanized surface by a direct nucleophilic substitution between free amines of the peptides (nucleophile) and chlorine atoms from the organofunctional groups of CPTES (leaving group) [65]. GL13K (GKIIKLKASLKLL-NH_2) has four lysines plus its N-terminus that are potential sites of immobilization; our previous work has shown that the antimicrobial activity of GL13K is insensitive to site-specificity [66]. To favor the surface orientation of MMP9-CP (KKGGGPLGMYS; cleavable at PLGMYS) at the N-terminus, we designed our peptide with two additional lysines - each one providing a potentially reacting free amine - like in previous work [24]. Three glycines were used as a spacer [60] between the lysines and the enzyme cleavable domain.

The co-immobilization of the mixed peptides was conducted in 9 different conditions; all combinations of three different solution pHs and three immobilization orders of adding the peptides in order to find

A

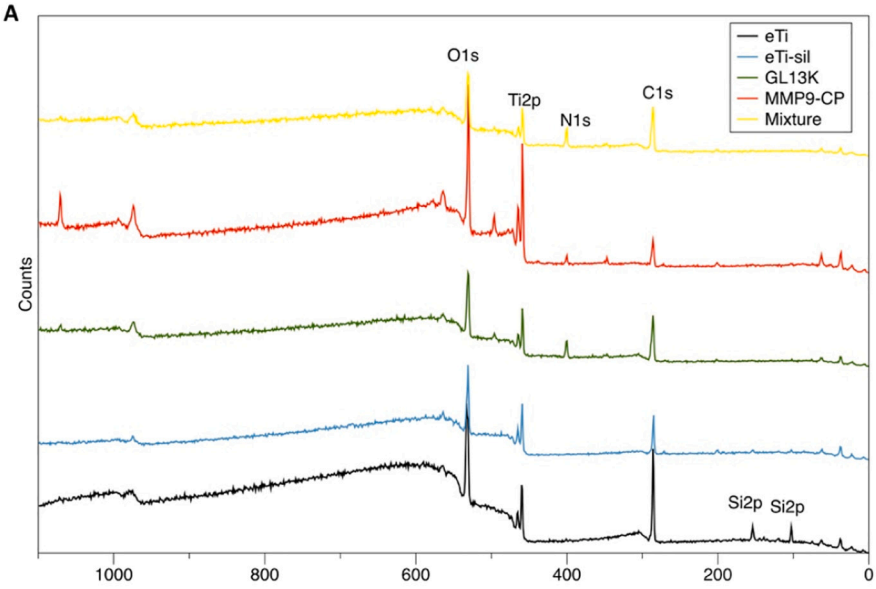

B

Surface	C1s	N1s	O1s	Si2p	Ti2p	N1s/Ti2p
eTi	12.40	0.00	61.22	3.76	22.62	0.00
eTi-sil	13.63	0.00	66.74	0.32	19.31	0.00
GL13K	41.23	12.30	37.84	0.00	8.63	1.44
MMP9-CP	46.40	11.21	35.29	0.12	6.98	1.61
Mixture	42.69	10.52	40.54	0.00	6.25	1.68

C

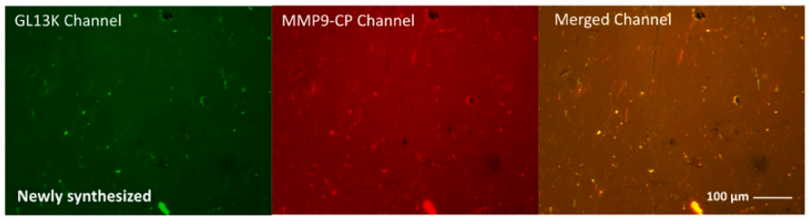

D

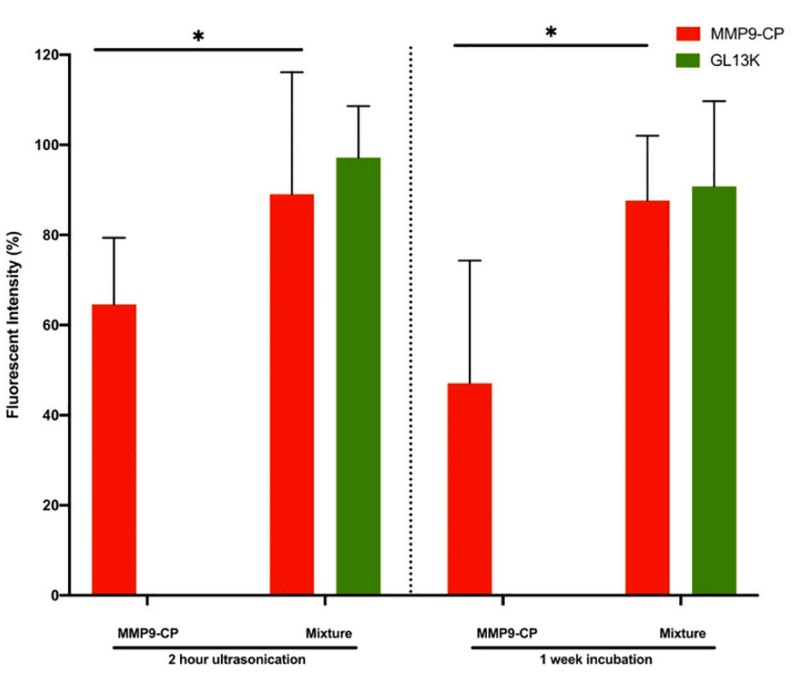

Fig. 2. Chemical analysis and stability of Mixture peptide coatings. (A) Chemical analysis (XPS) of immobilized peptides surfaces and controls (eTi and eTi-sil). B) XPS atomic % ratio (At.% ratio). (C) Fluorescent micrographs of co-immobilized peptide Mixture surfaces (GL13K: green, MMP9-CP:red, Merged:yellow). (D) Fluorescent intensity of mono-immobilized MMP9-CP and co-immobilized peptide Mixture surfaces after ultrasonication in deionized water for 2 h and incubation in DI water for one week at 37 °C compared as a percentage of newly synthesized surfaces. * denotes a statistically significant difference between MMP9-CP fluorescent intensities on mono-immobilized MMP9-CP vs. Mixture surfaces. (For interpretation of the references to colour in this figure legend, the reader is referred to the web version of this article.)

reaction conditions that favored balanced co-immobilization (Fig. 1B). pH was explored as a variable because charge can affect competitive electrostatic attraction/repulsion between GL13K and MMP9-CP as they move from solution to the CPTES-silanized surface [67]. The order of adding GL13K and MMP9-CP for immobilization was explored because adsorption and covalent attachment kinetics may differ between each peptide [68]. Surfaces co-immobilized with the peptides simultaneously showed red MMP9-CP dominating the surface leading to a weak GL13K green signal (Fig. 1E). Surfaces pre-immobilized with MMP9-CP for 3.5 h before adding GL13K again showed a weak GL13K signal (Fig. 1D). However, relatively similar signals were detected for both peptides (Fig. 1C) when surfaces were pre-immobilized with GL13K for 3.5 h before adding MMP9-CP. These results suggest MMP9-CP has a higher affinity to CPTES-silanized Ti surfaces than GL13K. GL13K has more lysines (four) in its sequence than MMP9-CP (only two lysines), which provide more amine groups to favor the nucleophilic immobilization reaction. However, the lysines in GL13K are scattered through the sequence (disregarding potential formation of secondary structures and/or supramolecular assemblies of either peptide in solution) while the lysines are clustered in the N-terminal of MMP9-CP; this clustering may cause a higher polarization of the MMP9-CP molecules that may favor the electrostatic attraction and, thus, immobilization of MMP9-CP over GL13K. Additionally, the MMP9-CP peptides contain fewer number of hydrophobic amino acids than the GL13K, rendering a more polar peptide, which has been shown as the preferential physical-chemical property governing adsorption of GL13K on solid substrates [69]. These factors may explain the need for GL13K pre-immobilization for a more "balanced" peptide co-immobilized coating. Solution pH might also influence the peptide co-immobilization. However, as the isoelectric points are rather similar between these two peptides (GL13K; pH = 11.01 and MMP9-CP; pH = 10.08), pH likely had a minor effect on the selection of the peptide preferentially immobilized on the silanized Ti surfaces. Results showed (Fig. 2A) relatively similar signals on pre-immobilized GL13K and MMP9-CP as well as simultaneously co-immobilized at each of three pHs. Within the pre-immobilized GL13K group, pH = 9.5 seemed to favor a balanced peptide co-immobilization. Therefore, the optimized condition for co-immobilization was selected as pH = 9.5 with surfaces pre-immobilized with GL13K ("Mixture" group henceforth).

3.2. Chemical characterization of multi-peptide mixture coating

XPS results confirmed the successful immobilization of the peptide coatings on Ti surfaces. A more detailed XPS analysis of mono-immobilized GL13K may be found in our previous work [23]. Fig. 2A shows the elemental composition of the treated surfaces (survey spectra). eTi surfaces revealed characteristic C1s (ca. 285 eV), Ti2p (ca. 460 eV) and O1s (ca. 530 eV) peaks. All of the surfaces with covalently immobilized peptides (GL13K, MMP9-CP, and Mixture) showed a strong nitrogen signal (N1s peak at ca. 400 eV) attributable to amino acids suggesting the successful immobilization of peptides on Ti surfaces. Quantification of XPS atomic % ratios (Fig. 2B) demonstrated a N1s/Ti2p ratio, again attributable to amino acids immobilized on a Ti surface, of between 1.44 and 1.68 for GL13K, MMP9-CP, and Mixture.

3.3. Mechanical stability of the multi-peptide mixture coating

In order to test the stability of the peptide coatings, we ultrasonicated the Mixture surface in distilled water for 2 h and re-examined the signal of fluorescently labeled peptides after this mechanical challenge. Fig. 2C demonstrates that newly synthesized surfaces produced both green (GL13K) and red (MMP9-CP) homogenous signals and the merging of those two showed yellowish images, as expected. Both green and red signal were strongly retained on the Mixture surface after ultrasonication (GL13K: 97.2 ± 11.4% and MMP9-CP: 89.09 ± 27.0% of newly synthesized) and incubation at 37 °C in DI water (GL13K: 90.8 ± 18.9% and MMP9-CP: 87.67 ± 14.36%) for one week, indicating the robust stability of both GL13K and MMP9-CP peptides (Fig. 2D), and again suggesting that sequential immobilization of the two different peptides did not hinder tethering of the second peptide, MMP9-CP in this case. Mono-immobilized MMP9-CP showed less stability (ultrasonication: 64.6 ± 14.8%; one week incubation: 47.11 ± 27.2%), suggesting the hydrophobic GL13K helps protect against peptide loss. This peptide loss is likely due to hydrolysis of the anchoring silane layer but further investigation is needed to confirm this [70]. Additional work is necessary to confirm peptide biological activity after incubation, although our past work has shown GL13K demonstrates antimicrobial potency after 18 days when adsorbed to dentin under incubation with a highly cariogenic biofilm [71].

3.4. Antimicrobial activity of the multi-peptide mixture coating

The antimicrobial activity of the mixture surfaces were evaluated with *S. gordonii*, a primary colonizer on oral surfaces that provides attachment for subsequent pathogenic biofilm formation by other species such as *Porphyromonas gingivalis* [72,73]. We selected a 24 h culture time based on past work that showed robust biofilm formation after this time period on control substrates [74–76]. *S. gordonii* has also been found in the microbiota of colonizing bacteria after dental implants surgery [77]. eTi, mono-immobilized GL13K, and MMP9-CP surfaces were used as controls. Our previous work has shown that GL13K possesses strong antimicrobial activity against *S. gordonii* [78]. Indeed, we have previously shown in a drip flow biofilm reactor, which enables in vitro simulation of some of the important conditions for bacteria biofilm development in vivo, GL13K immobilized on titanium is antimicrobial against *S. gordonii* after 3 days of culture [78]. Similarly, we showed GL13K retained antimicrobial activity when elastin-like recombinamers terminated with GL13K where immobilized on titanium and oral

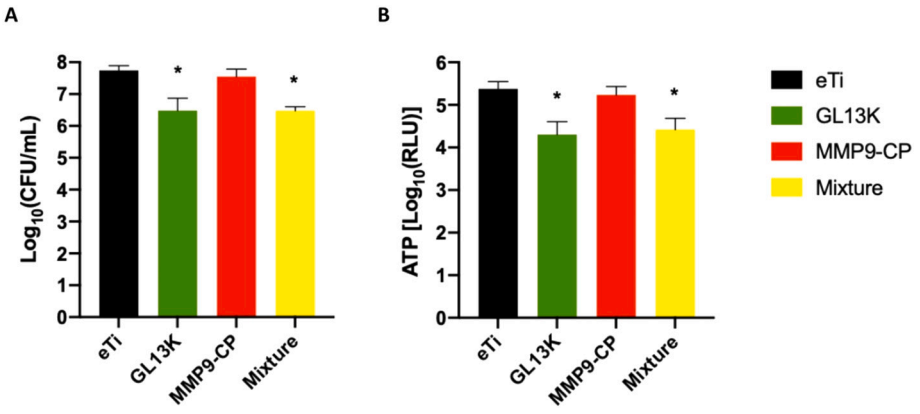

Fig. 3. Antimicrobial activity of Mixture peptide coatings against *S. gordonii.* (A) CFU/mL and (B) ATP RLU of control eTi, mono-peptide GL13K and MMP9-CP coatings and co-immobilized peptides Mixture coating. * denotes a statistically significant difference compared to eTi control.

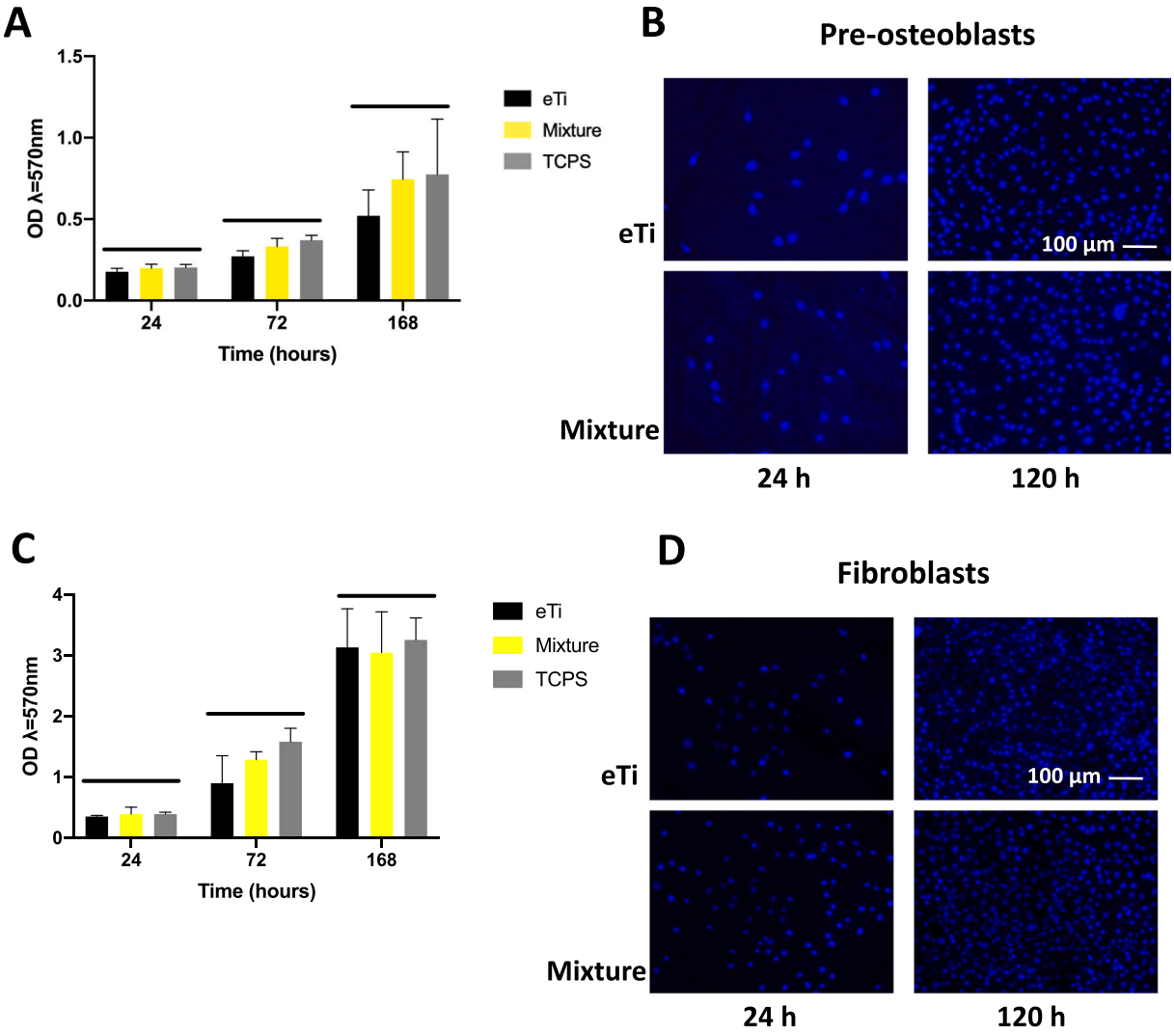

Fig. 4. Cytocompatibility of Mixture peptide coatings and control eTi and TCPS surfaces with pre-osteoblasts and fibroblasts. (A) Metabolic activity of pre-osteoblasts through 168 h. (B) Representative fluorescence micrographs of DAPI-stained pre-osteoblasts. (C) Metabolic activity of fibroblasts through 168 h. (D) Representative fluorescence micrographs of DAPI-stained fibroblasts. A bar denotes no statistically significant differences between groups at each timepoint.

microcosm biofilms were cultured in a drip flow biofilm reactor for 7 total days [79].

In this work (Fig. 3), we also observed the significantly reduced bacteria viability (shown by CFU values; Fig. 3A) and metabolism (shown by ATP values; Fig. 3B) on GL13K surfaces in comparison with eTi surfaces. Notably, the Mixture surface obtained comparable

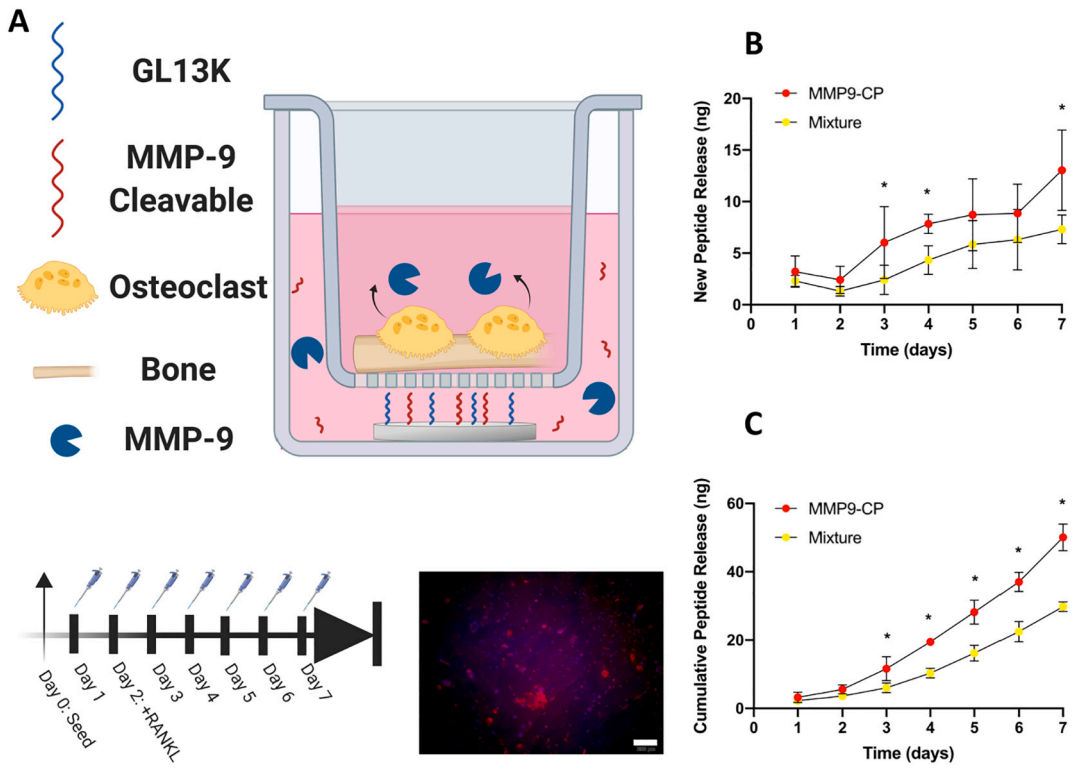

Fig. 5. Osteoclast-secreted MMP9-CP peptide release profile of mono-immobilized MMP9-CP and Mixture peptide coatings. (A) Schematic of experimental set-up culturing osteoclasts for endogenous MMP-9 secretion and representative MMP-9 osteoclast immunofluorescence at 7 days (DAPI is stained blue and MMP-9 is stained red; scale bar is 200 μm). (B) MMP9-CP release from mono-immobilized MMP9-CP and Mixture (ng peptide release since last time period per well) with background subtracted. (C) Cumulative MMP9-CP release of MMP9-CP mono-immobilized and Mixture (ng peptide release total per well) with background subtracted. * denotes a statistically significant difference between MMP9-CP and Mixture. (For interpretation of the references to colour in this figure legend, the reader is referred to the web version of this article.)

antimicrobial effect as mono-immobilized GL13K. On the other hand, mono-immobilized MMP9-CP did not display a significant antimicrobial effect, indicating the strong antimicrobial activity on the Mixture surface was exclusivity due to GL13K. This confirmed that a completely homogenous layer of GL13K (i.e., mono-immobilization) is not necessary for potent antimicrobial activity [80] and that co-immobilization did not hinder the activity of GL13K. Further work will be required to confirm these findings under more in vivo simulatory settings or in animal studies. Indeed, development of animal models for testing potency of antimicrobial materials/coatings is an unaddressed challenge in the field. Recent reviews [81,82] have noted the lack of guidelines and/or standards, "enormous" microbial dosing required to generate wounds in young animals, and under-powered models.

3.5. Cytocompatibility of the multi-peptide mixture coating

We next evaluated the cytocompatibility of our Mixture coating compared to eTi and tissue culture polystyrene (TCPS). Our long-term goal is multifunctional coatings with combined antimicrobial and enhanced bone regenerative activity triggered by active bone remodeling. As a result, we tested cytocompatibility using pre-osteoblasts (Fig. 4A and B) and fibroblasts (Fig. 4C and D) (as bone-anchored transdermal implants can come into contact surrounding soft tissues) [83] for up to 168 h (7 days) of culture. Our results showed no statistically significant differences in metabolic activity between Mixture surfaces compared to control eTi and TCPS for both pre-osteoblasts (Fig. 4A) and fibroblasts (Fig. 4C). DAPI-staining showed similar number of nuclei per field of view (Fig. 4B - pre-osteoblasts and Fig. 4D - fibroblasts) between groups with a clear increase in the number of cells in all groups from 24 to 120 h (5 days). These results are in agreement with our previous results for mono-immobilized GL13K[23] and overall suggest these coatings allow cellular proliferation and are cytocompatible to a similar extent as the gold-standard controls eTi and TCPS.

3.6. MMP9-CP release from multi-peptide mixture coating mediated by osteoclast secreted MMP-9

We measured the release profile of the MMP9-CP peptide carrying a fluorescent probe to prove the dynamic response of our MMP-9 sensitive, multifunctional surface, in the presence of MMP-9 secreted by osteoclasts. We used a transwell to culture osteoclasts on bone slices in the upper well to stimulate MMP-9 production to cleave MMP9-CP from mono-immobilized MMP9-CP and Mixture surfaces in the bottom well (Fig. 5A, top). We collected aliquots everyday post- seeding for up to a week, where osteoclast differentiation was initially stimulated at day 2 via the addition of RANKL (Fig. 5A, bottom left) [84]. The release profile of MMP-9 from osteoclasts is well described (increasing after RANKL addition toward a peak at 5 days; this corresponds to our day 7) [85] and we confirmed MMP-9 expression in our system at day 7 (Fig. 5A, bottom right). The release profile was plotted as new release since the previous timepoint (Fig. 5B) and as cumulative release (Fig. 5C) of mono-immobilized MMP9-CP and Mixture. A slight decrease in release between days 1 and 2 (Fig. 5B) suggests desorption of non-covalently sorbed peptides to the surface, perhaps from insufficient washing prior to testing. Both mono-immobilized MMP9-CP and Mixture showed similar release kinetics but we attribute the greater MMP9-CP release from mono-immobilized MMP9-CP to the presence of hydrophobic GL13K (which is hydrolytically and proteolytically stable) [86,87] likely inhibiting water penetration and enzyme accessibility to the Mixture surface. Mixture's lower release also likely relates to a lower overall surface loading of MMP9-CP on the mixture surface as it competes with GL13K for a finite number of chlorine atoms from the organofunctional

groups of CPTES on the surface. However, the reduced release of MMP9-CP on the mixture surface may benefit long-term delivery of the bioactive motif it carries (e.g. bone regenerative or immunomodulatory motif) to achieve extended release profiles.

Future work will focus on the conjugation of osteogenic and immunomodulatory motifs onto MMP9-CP for enhanced bone healing utilizing these release profiles. Possible candidates include Ln2-P3 (DLTIDDSYWYRI) [88], which enhances peri-implant bone regeneration [89,90], or angiopoietin-1 (QHREDGS) [91] which similarly stimulates osteogenic differentiation of osteoprogenitors when immobilized on Ti [92]. Immunomodulatory peptide candidates include the well-used RGD peptide that has an inhibitory effect on neutrophil chemotactic activity and phagocytic functionality and can reduce both phagocytosis and pro-inflammatory cytokine production in stimulated and unstimulated macrophages [93,94]. IDR-1018 [95], an otherwise antimicrobial peptide, is another possible candidate known to blunt macrophage proinflammatory cytokine production.

4. Conclusion

We have successfully engineered a dynamic, multi-functional peptide-based coating on titanium with antimicrobial and MMP-9 mediated release activity for synchronization of selected potential biological activities during bone remodeling. We envisage our coatings to reduce infection rates and overall enhance the success rates of all percutaneous, bone-anchored devices.

CRediT authorship contribution statement

Nicholas G. Fischer: Methodology, Formal analysis, Writing -original draft. **Xi Chen**: Conceptualization, Methodology, Formal analysis, Writing -original draft. **Kristina Astleford-Hopper**: Methodology, Formal analysis, Writing - review & editing. **Jiahe He:** Methodology, Formal analysis, Writing - review & editing. **Alex F. Mullikin**: Methodology, Formal analysis. **Kim C. Mansky**: Resources, Funding acquisition, Writing - review & editing. **Conrado Aparicio**: Conceptualization, Formal analysis, Resources, Funding acquisition, Supervision, Writing - review & editing.

Declaration of competing interest

The authors declare that they have no known competing financial interests or personal relationships that could have appeared to influence the work reported in this paper.

Acknowledgements

The authors would like to thank Dr. Jessica Jurovich, Dr. Christine B. Lung, and Professor Sven-Ulrik Gorr at the University of Minnesota for their training and support on experimental tasks for cell culturing, enzyme release, and antimicrobial characterization, respectively. We would also thank Professor Louis Mansky at the University of Minnesota for providing access to the multi-mode microplate reader. This project was supported by the Office of the Vice-president for Research at the University of Minnesota (Project #55466 of the Grant-in-Aid of Research, Artistry and Scholarship Program; CA), National Institute of Dental & Craniofacial Research (Grants R90DE023058 (XC) and T90DE0227232 (NGF and KA), and the Summer Dental Students Research Program of the University of Minnesota School of Dentistry (AFM). XC and NGF were also partially supported by a 3M Science and Technology Fellowship. Parts of this work were carried out in the Characterization Facility, University of Minnesota, which receives partial support from the NSF through the MRSEC (Award Number DMR-2011401) and the NNCI (Award Number ECCS-2025124) programs. Figures were created with BioRender (biorender.com).

References

[1] Gristina, A. G. Biomaterial-Centered Infection: Microbial adhesion versus tissue integration. Science 1987, 237 (4822), 1588–1595 DOI: https://doi.org/10.1126/science.3629258.
[2] Renvert, S.; Polyzois, I. Treatment of Pathologic Peri-Implant Pockets. *Periodontol. 2000* 2018, *76* (1), 180–190 DOI: https://doi.org/10.1111/prd.12149.
[3] G.L. Koons, M. Diba, A.G. Mikos, Materials design for bone-tissue engineering, Nat. Rev. Mater. 5 (8) (2020) 584–603, https://doi.org/10.1038/s41578-020-0204-2.
[4] R. Osman, M. Swain, A critical review of dental implant materials with an emphasis on titanium versus zirconia, Materials (Basel) 8 (3) (2015) 932–958, https://doi.org/10.3390/ma8030932.
[5] Zaid, M. B.; O'Donnell, R. J.; Potter, B. K.; Forsberg, J. A. Orthopaedic osseointegration. J. Am. Acad. Orthop. Surg. 2019, 27 (22), e977–e985 DOI: https://doi.org/10.5435/JAAOS-D-19-00016.
[6] A.L. Overmann, C. Aparicio, J.T. Richards, I. Mutreja, N.G. Fischer, S.M. Wade, B. K. Potter, T.A. Davis, J.E. Bechtold, J.A. Forsberg, D. Dey, Orthopaedic osseointegration: implantology and future directions, J. Orthop. Res. 38 (7) (2020) 1445–1454, https://doi.org/10.1002/jor.24576.
[7] J.C.M. Souza, M.B. Sordi, M. Kanazawa, S. Ravindran, B. Henriques, F.S. Silva, C. Aparicio, L.F. Cooper, Nano-scale modification of titanium implant surfaces to enhance osseointegration, Acta Biomater. 94 (2019) 112–131, https://doi.org/10.1016/j.actbio.2019.05.045.
[8] R. Liu, S. Chen, P. Huang, G. Liu, P. Luo, Z. Li, Y. Xiao, Z. Chen, Z. Chen, Immunomodulation-based strategy for improving soft tissue and metal implant integration and its implications in the development of metal soft tissue materials, Adv. Funct. Mater. 30 (21) (2020) 1910672, https://doi.org/10.1002/adfm.201910672.
[9] B.R. Chrcanovic, J. Kisch, T. Albrektsson, A. Wennerberg, A retrospective study on clinical and radiological outcomes of oral implants in patients followed up for a minimum of 20 years, Clin. Implant. Dent. Relat. Res. 20 (2) (2018) 199–207, https://doi.org/10.1111/cid.12571.
[10] Atallah, R.; Leijendekkers, R. A.; Hoogeboom, T. J.; Frölke, J. P. Complications of bone-anchored prostheses for individuals with an extremity amputation: a systematic review. PLoS One 2018, 13 (8), 0–3 DOI: https://doi.org/10.1371/journal.pone.0201821.
[11] H.W. Elani, J.R. Starr, J.D. Da Silva, G.O. Gallucci, Trends in dental implant use in the U.S., 1999–2016, and projections to 2026, J. Dent. Res. 97 (13) (2018) 1424–1430, https://doi.org/10.1177/0022034518792567.
[12] H. Schliephake, D. Scharnweber, Chemical and biological functionalization of titanium for dental implants, J. Mater. Chem. 18 (21) (2008) 2404–2414, https://doi.org/10.1039/b715355b.
[13] D. Zhang, X. Xu, X. Long, K. Cheng, J. Li, Advances in biomolecule inspired polymeric material decorated interfaces for biological applications, Biomater. Sci. 7 (10) (2019) 3984–3999, https://doi.org/10.1039/C9BM00746F.
[14] N.G. Fischer, E.A. Münchow, C. Tamerler, M.C. Bottino, C. Aparicio, Harnessing biomolecules for bioinspired dental biomaterials, J. Mater. Chem. B 8 (38) (2020) 8713–8747, https://doi.org/10.1039/D0TB01456G.
[15] J. Sharan, V. Koul, A.K. Dinda, O.P. Kharbanda, S.V. Lale, R. Duggal, M. Mishra, G. Gupta, M.P. Singh, Bio-functionalization of grade V titanium alloy with type I human collagen for enhancing and promoting human periodontal fibroblast cell adhesion – an in-vitro study, Colloids Surf. B. Biointerfaces 161 (2018) 1–9, https://doi.org/10.1016/j.colsurfb.2017.10.024.
[16] S. Acosta, L. Quintanilla, M. Alonso, C. Aparicio, J.C. Rodríguez-Cabello, Recombinant AMP/polypeptide self-assembled monolayers with synergistic antimicrobial properties for bacterial strains of medical relevance, ACS Biomater. Sci. Eng. 5 (9) (2019) 4708–4716, https://doi.org/10.1021/acsbiomaterials.9b00247.
[17] J.W. Dean, K.C. Culbertson, A.M. D'Angelo, Fibronectin and laminin enhance gingival cell attachment to dental implant surfaces in vitro, Int. J. Oral Maxillofac. Implant. 10 (6) (1995) 1–17.
[18] G. Vidal, T. Blanchi, A.J. Mieszawska, R. Calabrese, C. Rossi, P. Vigneron, J. L. Duval, D.L. Kaplan, C. Egles, Enhanced cellular adhesion on titanium by silk functionalized with titanium binding and RGD peptides, Acta Biomater. 9 (1) (2013) 4935–4943, https://doi.org/10.1016/j.actbio.2012.09.003.
[19] Middleton, C. A.; Pendegrass, C. J.; Gordon, D.; Jacob, J.; Blunn, G. W. Fibronectin Silanized Titanium Alloy: A Bioinductive and Durable Coating to Enhance Fibroblast Attachment in Vitro. *J. Biomed. Mater. Res. - Part A* 2007, *83* (4), 1032–1038 DOI: https://doi.org/10.1002/jbm.a.31382.
[20] Van Den Beucken, J. J. J. P.; Walboomers, X. F.; Vos, M. R. J.; Sommerdijk, N. A. J. M.; Nolte, R. J. M.; Jansen, J. A. Cyto- and Histocompatibility of Multilayered DNA-Coatings on Titanium. *J. Biomed. Mater. Res. - Part A* 2006, *77* (1), 202–211 DOI: https://doi.org/10.1002/jbm.a.30583.
[21] G. Yang, J. Zhang, W. Dong, L. Liu, J. Shi, H. Wang, Fabrication, characterization, and biological assessment of multilayer Laminin Γ2 DNA coatings on titanium surfaces, Sci. Rep. 6 (1) (2016) 23423, https://doi.org/10.1038/srep23423.
[22] E.C. Wisdom, Y. Zhou, C. Chen, C. Tamerler, M.L. Snead, Mitigation of peri-implantitis by rational design of bifunctional peptides with antimicrobial properties, ACS Biomater. Sci. Eng. 6 (5) (2020) 2682–2695, https://doi.org/10.1021/acsbiomaterials.9b01213.
[23] K.V. Holmberg, M. Abdolhosseini, Y. Li, X. Chen, S.U. Gorr, C. Aparicio, Bio-inspired stable antimicrobial peptide coatings for dental applications, Acta Biomater. 9 (9) (2013) 8224–8231.
[24] V.P. Koidou, P.P. Argyris, E.P. Skoe, J. Mota Siqueira, X. Chen, L. Zhang, J. E. Hinrichs, M. Costalonga, C. Aparicio, Peptide coatings enhance keratinocyte

attachment towards improving the peri-implant mucosal seal, Biomater. Sci. 6 (7) (2018) 1936–1945, https://doi.org/10.1039/c8bm00300a.
[25] M. Lucke, G. Schmidmaier, S. Sadoni, B. Wildemann, R. Schiller, N.P. Haas, M. Raschke, Gentamicin Coating of Metallic Implants Reduces Implant-Related Osteomyelitis in Rats 32, 2003, pp. 521–531, https://doi.org/10.1016/S8756-3282(03)00050-4.
[26] Riool, M.; Dirks, A. J.; Jaspers, V.; de Boer, L.; Loontjens, T. J. A.; van der Loos, C. M.; Florquin, S.; Apachitei, I.; Rijk, L. N. D.; Keul, H. A.; Zaat, S. A. J. A Chlorhexidine-Releasing Epoxy-Based Coating on Titanium Implants Prevents *Staphylococcus Aureus* Experimental Biomaterial-Associated Infection. *Eur. Cells Mater.* 2017, *33*, 143–157 DOI: 10.22203/eCM.v033a11.
[27] M. Diefenbeck, C. Schrader, F. Gras, T. Mückley, J. Schmidt, S. Zankovych, J. Bossert, K.D. Jandt, A. Völpel, B.W. Sigusch, H. Schubert, S. Bischoff, W. Pfister, B. Edel, M. Faucon, U. Finger, Gentamicin coating of plasma chemical oxidized titanium alloy prevents implant-related osteomyelitis in rats, Biomaterials 101 (2016) 156–164, https://doi.org/10.1016/j.biomaterials.2016.05.039.
[28] S.S. Zulfakar, J.D. White, T. Ross, M.L. Tamplin, Bacterial attachment to immobilized extracellular matrix proteins in vitro, Int. J. Food Microbiol. 157 (2) (2012) 210–217, https://doi.org/10.1016/j.ijfoodmicro.2012.05.007.
[29] L. Piroth, Y.A. Que, E. Widmer, A. Panchaud, S. Piu, J.M. Entenza, P. Moreillon, The fibrinogen- and fibronectin-binding domains of staphylococcus aureus fibronectin-binding protein A synergistically promote endothelial invasion and experimental endocarditis, Infect. Immun. 76 (8) (2008) 3824–3831, https://doi.org/10.1128/IAI.00405-08.
[30] K. Zhang, S. Wang, C. Zhou, L. Cheng, X. Gao, X. Xie, J. Sun, H. Wang, M.D. Weir, M.A. Reynolds, N. Zhang, Y. Bai, H.H.K. Xu, Advanced smart biomaterials and constructs for hard tissue engineering and regeneration, Bone Res. 6 (1) (2018) 31, https://doi.org/10.1038/s41413-018-0032-9.
[31] S. Ahadian, A. Khademhosseini, Smart scaffolds in tissue regeneration, Regen. Biomater. 5 (3) (2018) 125–128, https://doi.org/10.1093/rb/rby007.
[32] J. Zhang, X. Jiang, X. Wen, Q. Xu, H. Zeng, Y. Zhao, M. Liu, Z. Wang, X. Hu, Y. Wang, Bio-responsive smart polymers and biomedical applications, J. Phys. Mater. 2 (3) (2019), 032004, https://doi.org/10.1088/2515-7639/ab1af5.
[33] F. Khan, M. Tanaka, Designing smart biomaterials for tissue engineering, Int. J. Mol. Sci. 19 (1) (2018) 1–14, https://doi.org/10.3390/ijms19010017.
[34] A. Zamuner, P. Brun, M. Scorzeto, G. Sica, I. Castagliuolo, M. Dettin, Smart biomaterials: surfaces functionalized with proteolytically stable osteoblast-adhesive peptides, Bioact. Mater. 2 (3) (2017) 121–130, https://doi.org/10.1016/j.bioactmat.2017.05.004.
[35] Y. Akiyama, A. Kikuchi, M. Yamato, T. Okano, Ultrathin poly(N-isopropylacrylamide) grafted layer on polystyrene surfaces for cell adhesion/detachment control, Langmuir 20 (13) (2004) 5506–5511.
[36] K. Nagase, M. Yamato, H. Kanazawa, T. Okano, Poly(N -isopropylacrylamide)-based thermoresponsive surfaces provide new types of biomedical applications, Biomaterials 153 (2018) 27–48, https://doi.org/10.1016/j.biomaterials.2017.10.026.
[37] R. Dimitriou, E. Jones, D. McGonagle, P.V. Giannoudis, Bone regeneration: current concepts and future directions, BMC Med. 9 (1) (2011) 66, https://doi.org/10.1186/1741-7015-9-66.
[38] Y. Zhang, K. Hu, X. Xing, J. Zhang, M. Zhang, X. Ma, R. Shi, L. Zhang, Smart titanium coating composed of antibiotic conjugated peptides as an infection-responsive antibacterial agent, Macromol. Biosci. 2000194 (2020) 2000194, https://doi.org/10.1002/mabi.202000194.
[39] M. Abdolhosseini, S.R. Nandula, J. Song, H. Hirt, S.U. Gorr, Lysine substitutions convert a bacterial-agglutinating peptide into a bactericidal peptide that retains anti-lipopolysaccharide activity and low hemolytic activity, Peptides 35 (2) (2012) 231–238, https://doi.org/10.1016/j.peptides.2012.03.017.
[40] Brogden, K. A. Antimicrobial Peptides: Pore formers or metabolic inhibitors in bacteria? Nat. Rev. Microbiol. 2005, 3 (3), 238–250 DOI: https://doi.org/10.1038/nrmicro1098.
[41] S. Mai, M.T. Mauger, L. Niu, J.B. Barnes, S. Kao, B.E. Bergeron, J. Ling, F.R. Tay, Potential applications of antimicrobial peptides and their mimics in combating caries and pulpal infections, Acta Biomater. 49 (2017) 16–35, https://doi.org/10.1016/j.actbio.2016.11.026.
[42] S.J. Kridel, E. Chen, L.P. Kotra, E.W. Howard, S. Mobashery, J.W. Smith, Substrate hydrolysis by matrix metalloproteinase-9, J. Biol. Chem. 276 (23) (2001) 20572–20578, https://doi.org/10.1074/jbc.M100900200.
[43] M.D. Sternlicht, Z. Werb, How matrix metalloproteinases regulate cell behavior, Annu. Rev. Cell Dev. Biol. 17 (1) (2001) 463–516, https://doi.org/10.1146/annurev.cellbio.17.1.463.
[44] H. Birkedal-Hansen, W.G.I. Moore, M.K. Bodden, L.J. Windsor, B. Birkedal-Hansen, A. DeCarlo, J.A. Engler, Matrix metalloproteinases: a review, Crit. Rev. Oral Biol. Med. 4 (2) (1993) 197–250, https://doi.org/10.1177/10454411930040020401.
[45] J. Guo, H. Sun, W. Lei, Y. Tang, S. Hong, H. Yang, F.R. Tay, C. Huang, MMP-8-responsive polyethylene glycol hydrogel for intraoral drug delivery, J. Dent. Res. 98 (5) (2019) 564–571, https://doi.org/10.1177/0022034519831931.
[46] C. Chen, Y. Zhang, Z. Hou, X. Cui, Y. Zhao, H. Xu, Rational design of short peptide-based hydrogels with MMP-2 responsiveness for controlled anticancer peptide delivery, Biomacromolecules 18 (11) (2017) 3563–3571, https://doi.org/10.1021/acs.biomac.7b00911.
[47] B.E. Turk, L.L. Huang, E.T. Piro, L.C. Cantley, Determination of protease cleavage site motifs using mixture-based oriented peptide libraries, Nat. Biotechnol. 19 (7) (2001) 661–667, https://doi.org/10.1038/90273.
[48] A.H. Aziz, R.L. Wilmoth, V.L. Ferguson, S.J. Bryant, IDG-SW3 osteocyte differentiation and bone extracellular matrix deposition are enhanced in a 3D matrix metalloproteinase-sensitive hydrogel, ACS Appl. Bio Mater. 3 (3) (2020) 1666–1680, https://doi.org/10.1021/acsabm.9b01227.
[49] M. Steinhagen, P.G. Hoffmeister, K. Nordsieck, R. Hötzel, L. Baumann, M. C. Hacker, M. Schulz-Siegmund, A.G. Beck-Sickinger, Matrix metalloproteinase 9 (MMP-9) mediated release of MMP-9 resistant stromal cell-derived factor 1α (SDF-1α) from surface modified polymer films, ACS Appl. Mater. Interfaces 6 (8) (2014) 5891–5899, https://doi.org/10.1021/am500794q.
[50] L. Bai, J. Zhao, M. Wang, Y. Feng, J. Ding, Matrix-metalloproteinase-responsive gene delivery surface for enhanced in situ endothelialization, ACS Appl. Mater. Interfaces 12 (36) (2020) 40121–40132, https://doi.org/10.1021/acsami.0c11971.
[51] J. Christensen, V.P. Shastri, Matrix-metalloproteinase-9 is cleaved and activated by cathepsin K, BMC Res. Notes 8 (1) (2015) 1–8, https://doi.org/10.1186/s13104-015-1284-8.
[52] J. Gu, X.-S. Tong, G.-H. Chen, X.-Z. Liu, J.-C. Bian, Y. Yuan, Z.-P. Liu, Regulation of matrix metalloproteinase-9 protein expression by 1α,25-(OH) 2 D 3 during osteoclast differentiation, J. Vet. Sci. 15 (1) (2014) 133, https://doi.org/10.4142/jvs.2014.15.1.133.
[53] P.E. Purdue, P. Koulouvaris, B.J. Nestor, T.P. Sculco, The central role of wear debris in periprosthetic osteolysis, HSS J. 2 (2) (2006) 102–113, https://doi.org/10.1007/s11420-006-9003-6.
[54] C.-H. Tsai, Y.-J. Chen, F.-M. Huang, Y.-F. Su, Y.-C. Chang, The upregulation of matrix metalloproteinase-9 in inflamed human dental pulps, J. Endod. 31 (12) (2005) 860–862.
[55] C. Wang, Y. Liu, Y. Fan, X. Li, The use of bioactive peptides to modify materials for bone tissue repair, Regen. Biomater. 4 (3) (2017) 191–206, https://doi.org/10.1093/rb/rbx011.
[56] E. Jabbari, Osteogenic peptides in bone regeneration, Curr. Pharm. Des. 19 (19) (2013) 3391–3402, https://doi.org/10.2174/1381612811319190006.
[57] A. Vishwakarma, N.S. Bhise, M.B. Evangelista, J. Rouwkema, M.R. Dokmeci, A. M. Ghaemmaghami, N.E. Vrana, A. Khademhosseini, Engineering immunomodulatory biomaterials to tune the inflammatory response, Trends Biotechnol. 34 (6) (2016) 470–482, https://doi.org/10.1016/j.tibtech.2016.03.009.
[58] N. Marín-Pareja, E. Salvagni, J. Guillem-Marti, C. Aparicio, M.P. Ginebra, Collagen-functionalised titanium surfaces for biological sealing of dental implants: effect of immobilisation process on fibroblasts response, Colloids Surf. B. Biointerfaces 122 (2014) 601–610.
[59] X. Chen, P. Sevilla, C. Aparicio, Surface biofunctionalization by covalent co-immobilization of oligopeptides, Colloids Surf. B. Biointerfaces 107 (2013) 189–197, https://doi.org/10.1016/j.colsurfb.2013.02.005.
[60] J.A. Craig, E.L. Rexeisen, A. Mardilovich, K. Shroff, E. Kokkoli, Effect of linker and spacer on the design of a fibronectin-mimetic peptide evaluated via cell studies and AFM adhesion forces, Langmuir 24 (18) (2008) 10282–10292, https://doi.org/10.1021/la702434p.
[61] Fischer, N. G.; Aparicio, C. On the Proliferation of Cell Proliferation Tests. In *Handbook of Biomaterials Biocompatibility*; Mozafari, M., Ed.; Elsevier, 2020; pp. 175–193.
[62] N. Blixt, A. Norton, A. Zhang, C. Aparicio, H. Prasad, R. Gopalakrishnan, E. D. Jensen, K.C. Mansky, Loss of myocyte enhancer factor 2 expression in osteoclasts leads to opposing skeletal phenotypes, Bone 138 (2020) 115466, https://doi.org/10.1016/j.bone.2020.115466.
[63] A. Tasca, K. Astleford, N.C. Blixt, E.D. Jensen, R. Gopalakrishnan, K.C. Mansky, SMAD1/5 signaling in osteoclasts regulates bone formation via coupling factors, PLoS One 13 (9) (2018), e0203404, https://doi.org/10.1371/journal.pone.0203404.
[64] M.Y. Berezin, S. Achilefu, Fluorescence lifetime measurements and biological imaging, Chem. Rev. 110 (5) (2010) 2641–2684, https://doi.org/10.1021/cr900343z.
[65] Chen, X.; Li, Y.; Aparicio, C. Biofunctional Coatings for Dental Implants. In *Thin Films and Coatings in Biology*; 2013; pp. 105–143.
[66] C. Lan, A Multi-Functional St-ELR Scaffold for Dentin Regeneration, University of Minnesota, 2016.
[67] L. Betancor, H.R. Luckarift, Co-immobilized coupled enzyme systems in biotechnology, Biotechnol. Genet. Eng. Rev. 27 (1) (2010) 95–114, https://doi.org/10.1080/02648725.2010.10648146.
[68] P. Sevilla, J. Gil, C. Aparicio, Relevant properties for immobilizing short peptides on biosurfaces, IRBM 38 (5) (2017) 256–265, https://doi.org/10.1016/j.irbm.2017.06.003.
[69] Z. Ye, A.C. Kobe, T. Sang, C. Aparicio, Unraveling dominant surface physicochemistry to build antimicrobial peptide coatings with supramolecular amphiphiles, Nanoscale 12 (40) (2020) 20767–20775, https://doi.org/10.1039/D0NR04526H.
[70] S.R. Wasserman, Y.T. Tao, G.M. Whitesides, Structure and reactivity of alkylsiloxane monolayers formed by reaction of alkyltrichlorosilanes on silicon substrates, Langmuir 5 (4) (1989) 1074–1087, https://doi.org/10.1021/la00088a035.
[71] D.G. Moussa, C. Aparicio, Targeting the oral plaque microbiome with immobilized anti-biofilm peptides at tooth-restoration interfaces, PLoS One 15 (7) (2020), e0235283, https://doi.org/10.1371/journal.pone.0235283.
[72] How, K. Y.; Song, K. P.; Chan, K. G. Porphyromonas Gingivalis: An Overview of Periodontopathic Pathogen below the Gum Line. *Front. Microbiol.* 2016, *7* (FEB), 1–14 DOI: https://doi.org/10.3389/fmicb.2016.00053.
[73] G.S. Cook, J.W. Costerton, R.J. Lamont, Biofilm formation by porphyromonas gingivalis and streptococcus gordonii, J. Periodontal Res. 33 (6) (1998) 323–327, https://doi.org/10.1111/j.1600-0765.1998.tb02206.x.

[74] Z. Liu, S. Ma, S. Duan, D. Xuliang, Y. Sun, X. Zhang, X. Xu, B. Guan, C. Wang, M. Hu, X. Qi, X. Zhang, P. Gao, Modification of titanium substrates with chimeric peptides comprising antimicrobial and titanium-binding motifs connected by linkers to inhibit biofilm formation, ACS Appl. Mater. Interfaces 8 (8) (2016) 5124–5136, https://doi.org/10.1021/acsami.5b11949.
[75] G. Hazell, P.W. May, P. Taylor, A.H. Nobbs, C.C. Welch, B. Su, Studies of black silicon and black diamond as materials for antibacterial surfaces, Biomater. Sci. 6 (6) (2018) 1424–1432, https://doi.org/10.1039/C8BM00107C.
[76] R. Peyyala, S.S. Kirakodu, J.L. Ebersole, K.F. Novak, Novel model for multispecies biofilms that uses rigid gas-permeable lenses, Appl. Environ. Microbiol. 77 (10) (2011) 3413–3421, https://doi.org/10.1128/AEM.00039-11.
[77] M.M. Fürst, G.E. Salvi, N.P. Lang, G.R. Persson, Bacterial colonization immediately after installation on oral titanium implants, Clin. Oral Implants Res. 18 (4) (2007) 501–508, https://doi.org/10.1111/j.1600-0501.2007.01381.x.
[78] X. Chen, H. Hirt, Y. Li, S.-U. Gorr, C. Aparicio, Antimicrobial GL13K peptide coatings killed and ruptured the wall of streptococcus gordonii and prevented formation and growth of biofilms, PLoS One 9 (11) (2014), e111579, https://doi.org/10.1371/journal.pone.0111579.
[79] S. Acosta, A. Ibañez-fonseca, C. Aparicio, J.C. Rodriguez-Cabello, Antibiofilm coatings based on protein-engineered polymers and antimicrobial peptides for preventing implant-associated infections, Biomater. Sci. 22 (3) (2020) 154, https://doi.org/10.1039/D0BM00155D.
[80] N.G. Fischer, D.G. Moussa, E.P. Skoe, D.A. De Jong, C. Aparicio, Keratinocyte-specific peptide-based surfaces for hemidesmosome upregulation and prevention of bacterial colonization, ACS Biomater. Sci. Eng. 6 (9) (2020) 4929–4939, https://doi.org/10.1021/acsbiomaterials.0c00845.
[81] Moriarty, T. F.; Grainger, D. W.; Richards, R. G. Challenges in Linking Preclinical Anti-Microbial Research Strategies with Clinical Outcomes for Device-Associated Infections. *Eur. Cells Mater.* 2014, *28*, 112–128 DOI: 10.22203/eCM.v028a09.
[82] Kreth, J.; Merritt, J.; Pfeifer, C. S.; Khajotia, S.; Ferracane, J. L. Interaction between the Oral Microbiome and Dental Composite Biomaterials: Where We Are and Where We Should Go. J. Dent. Res. 2020, 002203452092769 DOI: https://doi.org/10.1177/0022034520927690.
[83] Esposito, M.; Maghaireh, H.; Grusovin, M. G.; Ziounas, I.; Worthington, H. V. Soft Tissue Management for Dental Implants: What Are the Most Effective Techniques? A Cochrane Systematic Review. *Eur. J. Oral Implantol.* 2012, *5* (3), 221–238 DOI: 23000707.
[84] Park, J. H.; Lee, N. K.; Lee, S. Y. Current Understanding of RANK Signaling in Osteoclast Differentiation and Maturation. *Mol. Cells* 2017, *40* (10), 706–713 DOI: 10.14348/molcells.2017.0225.
[85] Zhu, L.; Tang, Y.; Li, X.; Keller, E. T.; Yang, J.; Cho, J.; Feinberg, T. Y.; Weiss, S. J. Osteoclast-Mediated Bone Resorption Is Controlled by a Compensatory Network of Secreted and Membrane-Tethered Metalloproteinases. *Sci. Transl. Med.* 2020, *12* (529), eaaw6143 DOI: https://doi.org/10.1126/scitranslmed.aaw6143.
[86] X. Chen, Multi-Bioactive Peptide Coatings for Dental Implants - PhD Dissertation, University of Minnesota School of Dentistry, 2014.
[87] D.G. Moussa, A. Fok, C. Aparicio, Hydrophobic and antimicrobial dentin: a peptide-based 2-tier protective system for dental resin composite restorations, Acta Biomater. 88 (2019) 251–265, https://doi.org/10.1016/j.actbio.2019.02.007.
[88] S.Y. Jung, J.-M. Kim, H.K. Kang, D.H. Jang, B.-M. Min, A biologically active sequence of the Laminin A2 large globular 1 domain promotes cell adhesion through Syndecan-1 by inducing phosphorylation and membrane localization of protein kinase Cδ, J. Biol. Chem. 284 (46) (2009) 31764–31775, https://doi.org/10.1074/jbc.M109.038547.
[89] H.K. Kang, O.B. Kim, S.K. Min, S.Y. Jung, D.H. Jang, T.K. Kwon, B.M. Min, I.S. Yeo, The effect of the DLTIDDSYWYRI motif of the human Laminin A2 chain on implant osseointegration, Biomaterials 34 (16) (2013) 4027–4037, https://doi.org/10.1016/j.biomaterials.2013.02.023.
[90] Choi, J.; Kim, S.; Jo, S. Bin; Kang, H. K.; Jung, S. Y.; Kim, S. W.; Min, B.; Yeo, I. L. A Laminin-211-derived Bioactive Peptide Promotes the Osseointegration of a Sandblasted, Large-grit, Acid-etched Titanium Implant. *J. Biomed. Mater. Res.* Part A 2020, 108 (5), 1214–1222 DOI: https://doi.org/10.1002/jbm.a.36895.
[91] Dallabrida, S. M.; Ismail, N.; Oberle, J. R.; Himes, B. E.; Rupnick, M. A. Angiopoietin-1 Promotes Cardiac and Skeletal Myocyte Survival Through Integrins. *Circ. Res.* 2005, *96* (4) DOI: https://doi.org/10.1161/01.RES.0000158285.57191.60.
[92] N.T. Feric, C.C.H. Cheng, M.C. Goh, V. Dudnyk, V. Di Tizio, M. Radisic, Angiopoietin-1 peptide QHREDGS promotes osteoblast differentiation, bone matrix deposition and mineralization on biomedical materials, Biomater. Sci. 2 (10) (2014) 1384–1398, https://doi.org/10.1039/C4BM00073K.
[93] R.M. Senior, H.D. Gresham, G.L. Griffin, E.J. Brown, A.E. Chung, Entactin stimulates neutrophil adhesion and chemotaxis through interactions between its Arg-Gly-asp (RGD) domain and the leukocyte response integrin, J. Clin. Invest. 90 (6) (1992) 2251–2257, https://doi.org/10.1172/JCI116111.
[94] A.T. Rowley, R.R. Nagalla, S.W. Wang, W.F. Liu, Extracellular matrix-based strategies for immunomodulatory biomaterials engineering, Adv. Healthc. Mater. 8 (8) (2019) 1–18, https://doi.org/10.1002/adhm.201801578.
[95] H. Choe, A.S. Narayanan, D.A. Gandhi, A. Weinberg, R.E. Marcus, Z. Lee, R. A. Bonomo, E.M. Greenfield, Immunomodulatory peptide IDR-1018 decreases implant infection and preserves osseointegration, Clin. Orthop. Relat. Res. 473 (9) (2015) 2898–2907, https://doi.org/10.1007/s11999-015-4301-2.